

# Color Constancy by Derivative-based Gamut Mapping

Arjan Gijsenij and Theo Gevers

University of Amsterdam

Kruislaan 403, 1098 SJ Amsterdam, The Netherlands

{gijsenij, gevers}@science.uva.nl

Joost van de Weijer

LEAR TEAM, GRAVIR INRIA

655, avenue de l'Europe, 38330 Montbonnet, France

joost.van-de-weijer@inrialpes.fr

## Abstract

*Color constancy aims to compute object colors despite differences in the color of the light source. Gamut-based approaches are very promising methods to achieve color constancy. In this paper, the gamut mapping approach is extended to incorporate higher-order statistics (derivatives) to estimate the illuminant.*

*A major problem of gamut mapping is that in case of a failure of the diagonal model no solutions are found, and therefore no illuminant estimation is performed. Image value offsets are often used to model deviations from the diagonal model. Prior work which incorporated robustness to offsets for gamut mapping assumed a constant offset over the whole image. In contrast to previous work, we model these offsets to be position dependent, and show that for this case derivative-based gamut mapping yields a valid solution to the illuminant estimation problem.*

*Experiments on both synthetic data and images taken under controlled laboratory settings reveal that the derivative-based and regular gamut mapping methods provide similar performance. However, the derivative-based method outperforms other methods on the more challenging task of color constancy for real-world images.*

## 1. Introduction

Differences in illumination cause measurements of object colors to be biased towards the color of the light source. Fortunately, humans have the ability of color constancy: they perceive the same color of an object despite large differences in illumination. A similar color constancy capability is necessary for various computer vision tasks such as object recognition, video retrieval and scene classification.

In this way, the extracted image features are only dependent on the colors of the objects. This is beneficial for the task at hand [15].

Many color constancy algorithms have been proposed, see [16] for a recent overview. Two widely used algorithms make use of simple statistics of the image to estimate the color of the illuminant. One is based on the assumption that the average color in a scene is achromatic (called the *Grey-World assumption* [4]), while the other assumes that the maximum response in a scene is caused by a perfect reflectance (called the *White-Patch assumption* [18]). Similar methods are the *Shades of Grey* algorithm [12], which actually embodies the *Grey-World* and the *White-Patch* algorithms as special cases, and the *Grey-Edge* algorithm [20]. Algorithms that use more advanced statistical information of the image, acquired in a learning phase, include probabilistic methods [3, 6] and gamut-based methods [9, 10, 14]. Gamut-based methods are very promising algorithms to achieve color constancy with high accuracy. Therefore, in this paper, we focus on gamut mapping.

Gamut mapping algorithms are restricted to the use of pixel values to estimate the illuminant. As a consequence, higher-order statistics in images are ignored. Recent work by Van de Weijer and Gevers [20] used image derivatives to improve color constancy. The *Grey-World* algorithm was extended to incorporate derivative information, resulting in the *Grey-Edge* algorithm, and this extension was shown to outperform current state-of-the-art methods. Consequently, the aim of this paper is to incorporate derivative information into more sophisticated approaches such as the gamut mapping approach.

Incorporation of derivative information has several advantages over the direct use of pixel values. Image derivatives are invariant with respect to an offset of the RGB values. Shafer [19] models diffuse light by adding such an off-



set to the (R,G,B)-values of the image. Diffuse light is a disturbing factor in real-world images as it occurs both in outdoor scenes (e.g. blue light coming from the sky) and in indoor scenes (e.g. light (inter)reflected by walls, ceilings and nearby objects). Furthermore, Finlayson *et al.* [11] use this offset to model slight deviations from the diagonal model, since the assumptions underlying the diagonal model (e.g. narrow-band filters) are not always satisfied. Both diffuse lighting and deviations from the diagonal model can degrade the performance of gamut mapping algorithms. The novelty of this paper is a derivative-based method using the elegance of the gamut mapping approach with additional robustness of the image derivatives to deviations of the diagonal model and diffuse lightning.

The paper is organized as follows. In sections 2 and 3, color constancy is defined and the original gamut mapping is explained, respectively. In section 4, the derivative-based gamut mapping algorithm is proposed. In sections 5 and 6, the experimental results and the conclusions are presented.

## 2. Color Constancy

### 2.1. Reflection model

An image  $\mathbf{f}$  can be modelled under the assumption of Lambertian reflectance as follows:

$$\mathbf{f}(\mathbf{x}) = \int_{\omega} e(\lambda)\rho_k(\lambda)s(\mathbf{x}, \lambda)d\lambda, \quad (1)$$

where  $e(\lambda)$  is the color of the light source,  $s(\mathbf{x}, \lambda)$  is de surface reflectance and  $\rho_k(\lambda)$  is the camera sensitivity function ( $k \in \{R, G, B\}$ ). Further,  $\omega$  and  $\mathbf{x}$  are the visible spectrum and the spatial coordinates respectively.

Shafer [19] proposes to add a "diffuse" light term to the model of eq. (1). The diffuse light is considered to have a lower intensity and to be coming from all directions in an equal amount:

$$\mathbf{f}(\mathbf{x}) = \int_{\omega} e(\lambda)\rho_k(\lambda)s(\mathbf{x}, \lambda)d\lambda + \int_{\omega} a(\lambda)\rho_k(\lambda), \quad (2)$$

where  $a(\lambda)$  is the term that models the diffuse light. Using this equation, objects under daylight should be better modelled, since daylight consists of both a point source (the sun) and diffuse light coming from the sky. Shafer does remark, however, that the assumption that diffuse light is equal in all directions, is highly idealized. A more realistic approximation would consider the diffuse light to be dependent on the position in the image, according to:

$$\mathbf{f}(\mathbf{x}) = \int_{\omega} e(\lambda)\rho_k(\lambda)s(\mathbf{x}, \lambda)d\lambda + \int_{\omega} \overline{a(\mathbf{x}, \lambda)}\rho_k(\lambda), \quad (3)$$

where we assume the dependence of the position to be low-frequency as indicated by the overline. This model falls short

to model the real nature of light-reflections and interactions of diffuse light and object reflections, however it allows to model the real world closer than eq. (2).

By assuming that the color of the light source  $\mathbf{e}$  depends on the color of the light source  $e(\lambda)$  as well as the camera sensitivity function  $\rho_k(\lambda)$ , color constancy is then equivalent to the estimation of  $\mathbf{e}$ :

$$\mathbf{e} = \int_{\omega} e(\lambda)\rho_k(\lambda)d\lambda. \quad (4)$$

Since, in general, only the image values of  $\mathbf{f}$  are known, this is an under-constrained problem, and it therefore can not be solved without further assumptions.

### 2.2. Diagonal model

Color constancy can be reached by determining the color of the illuminant of an input image. However, in many cases the color of the light source is of less importance than the appearance of the input image under a reference light. The aim of many color constancy applications is to transform all colors of the input image, taken under an unknown light source, to colors as they would appear under a reference light. This transformation can be modeled by a diagonal mapping or *von Kries Model* [21]. The diagonal mapping is given as follows:

$$\mathbf{f}^c = \mathcal{D}^{u,c}\mathbf{f}^u, \quad (5)$$

where  $\mathbf{f}^u$  is the image taken under an unknown light source,  $\mathbf{f}^c$  is the same image transformed, so it appears if it was taken under the reference light (called canonical illuminant), and  $\mathcal{D}^{u,c}$  is a diagonal matrix which maps colors that are taken under an unknown light source  $u$  to their corresponding colors under the canonical illuminant  $c$ :

$$\begin{pmatrix} R^c \\ G^c \\ B^c \end{pmatrix} = \begin{pmatrix} \alpha & 0 & 0 \\ 0 & \beta & 0 \\ 0 & 0 & \gamma \end{pmatrix} \begin{pmatrix} R^u \\ G^u \\ B^u \end{pmatrix} \quad (6)$$

However, under some conditions, the diagonal model is too strict, and no solutions are found (this situation is called the null solution problem). This could be caused by saturated colors or the presence of surfaces that were not represented in the canonical gamut. To overcome this, Finlayson *et al.* [11] accounted for the failure of the diagonal model by adding an offset term to the diagonal model, resulting in the diagonal-offset model:

$$\begin{pmatrix} R^c \\ G^c \\ B^c \end{pmatrix} = \begin{pmatrix} \alpha & 0 & 0 \\ 0 & \beta & 0 \\ 0 & 0 & \gamma \end{pmatrix} \begin{pmatrix} R^u \\ G^u \\ B^u \end{pmatrix} + \begin{pmatrix} o_1 \\ o_2 \\ o_3 \end{pmatrix} \quad (7)$$

Deviations from the diagonal model are reflected in the offset term  $(o_1, o_2, o_3)^T$ . Ideally, this term will be zero, which is the case when the diagonal model is valid.

Interestingly, the diagonal model also takes diffuse lighting into account as approximated by eq. (2). To take however position dependent diffuse lighting of eq. (3) into account extend the model to:

$$\begin{pmatrix} R^c \\ G^c \\ B^c \end{pmatrix} = \begin{pmatrix} \alpha & 0 & 0 \\ 0 & \beta & 0 \\ 0 & 0 & \gamma \end{pmatrix} \begin{pmatrix} R^u \\ G^u \\ B^u \end{pmatrix} + \begin{pmatrix} \overline{o_1(\mathbf{x})} \\ \overline{o_2(\mathbf{x})} \\ \overline{o_3(\mathbf{x})} \end{pmatrix} \quad (8)$$

In conclusion, eq. (8) can be used to overcome deviations from the diagonal model and diffuse light (assuming the dependence of the position is low-frequency).

### 3. Gamut Mapping

The gamut mapping algorithm has been introduced by Forsyth [14]. It is based on the assumption, that *in real-world images, for a given illuminant, one observes only a limited number of colors*. Consequently, any variation in the colors of an image (*i.e.* colors that are different from the colors that can be observed under a given illuminant) are caused by a deviation in the color of the light source.

The first stage of the algorithm is to find this limited set of colors that can occur under a given illuminant. This set is called the *canonical gamut*  $\mathcal{C}$  and is found by observing as many surfaces under one known light source (called the *canonical illuminant*) as possible.

The next stage, where the illuminant of an input image (taken under an unknown light source) is to be estimated, consists of three important steps:

1. Estimate the gamut of the unknown light source by assuming that the colors in the input image are representative for the gamut of the unknown light source. So, all colors of the input image are collected in the input gamut  $\mathcal{I}$ .
2. Determine the set of *feasible mappings*  $\mathcal{M}$ , *i.e.* all mappings that can be applied to the gamut of the input image and that result in a gamut that lies completely within the canonical gamut. Under the assumption of the diagonal mapping, a unique mapping exists that takes the gamut of the unknown light source to the canonical gamut. However, since the gamut of the unknown light source is simply estimated by using the gamut of *one* input image, in practice several mappings exist. Every mapping  $i$  in the set  $\mathcal{M}$  should take the input gamut completely inside the canonical gamut:

$$\mathcal{M}_i \mathcal{I} \in \mathcal{C}. \quad (9)$$

3. Apply an estimator to select one mapping from the set of feasible mappings. The selected mapping can be applied to the canonical illuminant to obtain an estimate of the unknown illuminant. The original method

[14] used the heuristic that the mapping resulting in the most colorful scene, *i.e.* the diagonal matrix with the largest trace, is the most suitable mapping. Alternatives are to use the average of the feasible set or a weighted average [1].

These are the basic steps of the gamut mapping algorithm. Several modifications have been proposed. Difficulties in implementation are addressed in [7, 8], where it was shown that the gamut mapping algorithm can also be computed in chromaticity space  $(\frac{R}{B}, \frac{G}{B})$ . However, the performance of this 2D approach is a slightly lower than the performance of the 3D approach. Dependency on the diagonal model is addressed in [1], where the canonical gamut is systematically enlarged by accounting for deviation of the diagonal model. In [11] the diagonal-offset model is introduced to account for diffuse light. Further, in [10] the problem of illuminant estimation is effectively reduced to the problem of *illuminant classification*.

### 4. Derivative-based Gamut Mapping

As discussed above, gamut mapping is based on the assumption that only limited set of colors are observed under a certain illuminant. Multiple phenomena in nature, such as zooming out, can cause the mixture colors. Therefore, if two colors are seen under a certain illuminant, then also all colors in between could be observed under this illuminant, since the set of all possible colors which can be seen under a certain illuminant form a convex hull (*i.e.* gamut). In this paper the gamut theory is extended by noting that the above is not only true for *image values* but also for every *linear combination of image values*. Hence, the correct estimate of an illuminant will also map every gamut which is constructed by a linear combination of image values back into the canonical gamut constructed with the same linear operation. In this paper, one such linear combination will be examined in more detail, namely image derivatives, which have some nice properties we will discuss in the following.

At the basis of the work of Forsyth [14] is eq. (1), in which an image  $\mathbf{f}$  is composed of the color of the light source  $e(\lambda)$ , the camera sensitivity function  $\rho_k(\lambda)$ , and the surface reflectance properties  $s(\mathbf{x}, \lambda)$ . The effect of diffuse light on the formation of an image can be modelled by adding an offset term (eq. (2)). By computing the derivative of image  $\mathbf{f}$ , it can be easily derived that the effect of the diffuse light source  $a(\lambda)$  is cancelled out, since it is independent of the surface reflectance term. Furthermore, if we assume the diffuse lighting to be low frequent (*i.e.* it is constant over the size of the derivative filter), derivative-based gamut mapping is also invariant to location-dependent offsets as modelled by eq. (3). Then, the reflection model of the spatial derivative of  $\mathbf{f}$  at location  $\mathbf{x}$  on scale  $\sigma$  is given

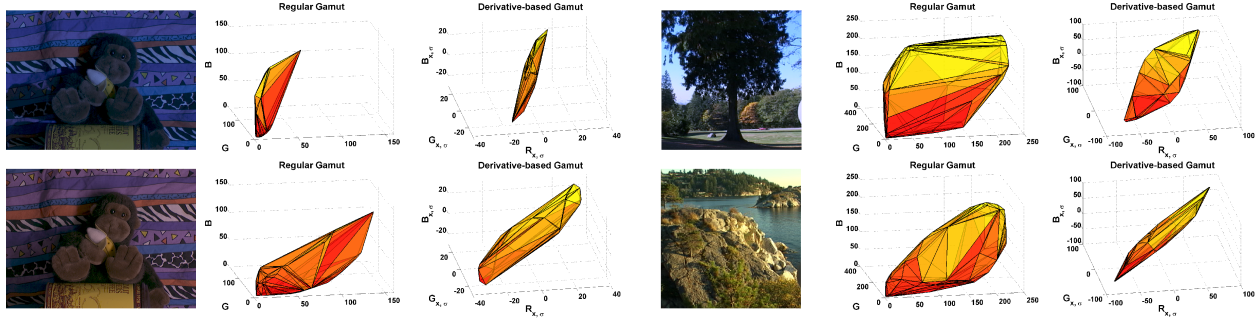


Figure 1. Examples of the regular gamut and the gamut of the derivatives of several scenes. The images of the monkey are taken from [2], and the real-world images are taken from [5]. From these images, it can be seen that the regular gamuts as well as the gamuts of the derivatives have discriminative power, and are different from each other.

by:

$$\mathbf{f}_{\mathbf{x},\sigma}(\mathbf{x}) = \int_{\omega} e(\lambda) \rho_k(\lambda) \mathbf{s}_{\mathbf{x},\sigma}(\mathbf{x}, \lambda) d\lambda. \quad (10)$$

Next, equivalently to [14], the orthonormal basis  $\{\phi_m(\lambda), 0 \leq m \leq L-1\}$  is considered for the space spanned by  $e^c(\lambda) \rho_k(\lambda)$ , where  $L$  denotes the number of receptors and  $e^c(\lambda)$  is the canonical illuminant:

$$e^c(\lambda) \rho_k(\lambda) = \sum_{j=0}^{j=L-1} a_{kj} \phi_j(\lambda). \quad (11)$$

Using this basis, a mapping  $\mathcal{M}^{c,u}$  which takes an image taken under the canonical illuminant  $c$  to its appearance under the unknown light source  $u$  can be recovered:

$$\begin{aligned} \mathcal{M}_k^{c,u} &= \sum_{i=0}^{i=L-1} \sum_{j=0}^{j=L-1} r_{kj}(u) a_{ji} \phi_i(\lambda) \\ &\times \int \mathbf{s}_{\mathbf{x},\sigma}(\mathbf{x}, \lambda) d\lambda \\ &+ \int F_k(\lambda, u) \mathbf{s}_{\mathbf{x},\sigma}(\mathbf{x}, \lambda), \end{aligned} \quad (12)$$

where  $F_k(\lambda, u)$  is a residue orthogonal to all the basis  $\phi_m(\lambda)$ . Now by expanding the surface reflectance in terms of the basis, a unique decomposition for any  $\mathbf{s}_{\mathbf{x},\sigma}(\mathbf{x}, \lambda)$  can be found:

$$\mathbf{s}_{\mathbf{x},\sigma}(\mathbf{x}, \lambda) = \sum_{i=0}^{i=L-1} \pi_i(\mathbf{x}) \phi_i(\lambda) + \mathbf{s}_{\mathbf{x},\sigma}^*(\mathbf{x}, \lambda), \quad (13)$$

where  $\mathbf{s}_{\mathbf{x},\sigma}^*(\lambda)$  is a residue. Using the above formulation, a *color constancy equation based on image derivatives*, similar to the one proposed by Forsyth, can be derived:

$$\begin{aligned} \mathcal{M}_k^{c,u} &= \sum_{i=0}^{i=L-1} \sum_{j=0}^{j=L-1} r_{ki}(u) a_{ij} \pi_j \\ &+ \int F_k(\lambda, u) \mathbf{s}_{\mathbf{x},\sigma}^*(\lambda) d\lambda. \end{aligned} \quad (14)$$

Under the minimal assumption of the first kind (*i.e.* constraining the illuminant such that the residual terms are zero), the residual term  $F_k(\lambda, u)$  is set to zero and the unknown light source  $u$  can be found by applying a version of the coefficient rule.

During the construction of the gamuts (both the canonical gamut and the input gamut), one should make sure that the transitions that are captured in the gamut are symmetric (*e.g.* if a transition from surface  $a$  to surface  $b$  is found, then the transition from surface  $b$  to surface  $a$  should also be in the gamut). Examples of the regular gamut and the gamut of the derivatives of several images are shown in figure 1. From these images, it can be seen that both the regular gamut and the derivative-based gamut contain discriminative power. Both the regular gamuts and the derivative-based gamuts of the images are completely different, even though the images are similar in content. Finally, it should be noted that the diagonal model can consist of strictly positive elements only.

## 5. Experiments

This section considers an empirical evaluation of the proposed algorithm. Although the proposed method is suited to include higher order derivatives (*e.g.*  $2^{nd}$ -nd order), in the experiments the focus is on first order derivatives *i.e.* edges. Edges are computed by a Gaussian derivative with  $\sigma = 3$ .

First, experiments are performed on synthetic data, resulting in a systematic analysis of the derivative-based gamut mapping. Then, experiments on real-world images are conducted.

### 5.1. Performance measure

For all images in the data set (both synthetic and real-world images), the correct color of the light source  $\mathbf{e}_l$  is known *a priori*. To measure how close the estimated illuminant resembles the true color of the light source, the angular

error  $\epsilon$  is used:

$$\epsilon = \cos^{-1}(\hat{\mathbf{e}}_l \cdot \hat{\mathbf{e}}_e), \quad (15)$$

where  $\hat{\mathbf{e}}_l \cdot \hat{\mathbf{e}}_e$  is the dot product of the two normalized vectors representing the true color of the light source  $\mathbf{e}_l$  and the estimated color of the light source  $\mathbf{e}_e$ . To provide more insight in the evaluation, the median as well as the mean angular error will be reported [17].

## 5.2. Synthetical data

Two experiments are conducted. In the first experiment, outlined in section 5.2.1, the performance of the different gamut mapping algorithms is tested as a function of the number of surfaces (edges). The second experiment, presented in section 5.2.2, focuses on the robustness of the methods against deviations from the diagonal model and diffuse light, modelled by simulating an offset in the diagonal model. We take the offset to be constant over the image.

The data set used is constructed by Barnard *et al.* [2], and consists of 1995 spectra taken from several sources. A synthetic data set is created by combining  $n$  spectra with one illuminant (chosen from a data set of 287 feasible illuminants, also from [2]). Using eq. (1), an illuminant-dependant  $(R, G, B)$ -value can be constructed from a surface reflectance spectrum, an illuminant spectrum and the (known) camera sensitivity function.

For the regular gamut mapping algorithm,  $(R, G, B)$ -values are used as the input of the algorithm. However, the derivative-based gamut mapping is concerned with derivatives. In the experiments, we focus on 1<sup>th</sup>-order statistics *i.e.* edges. An edge is defined as the difference between two  $(R, G, B)$ -values. Note that a scene with  $n$  different surfaces can contain several edges. However, the lower bound on the number of different edges for a scene containing  $n$  different surfaces is  $n - 1$ . The upper bound on the number of edges can be determined by computing all possible edges from one surfaces to another: for  $n$  surfaces, a total number of  $\frac{1}{2}n(n - 1)$  different edges occur, where it is assumed that an transition from surface  $a$  to surface  $b$  is identical to an transition from surface  $b$  to surface  $a$ .

### 5.2.1 Number of surfaces

The first experiment is concerned with computing the color constancy performance as function of the number of surfaces (or edges). Surfaces are randomly selected from the database of surface reflectance spectra. To compare the performance of the regular gamut mapping with the derivative-based gamut mapping algorithm, two different number of edges are created for each scene: the lower bound and the upper bound. Along with a randomly selected illuminant from the database of illuminants, a synthetic data set is created containing  $n$   $(R, G, B)$ -values, and  $n - 1$  and

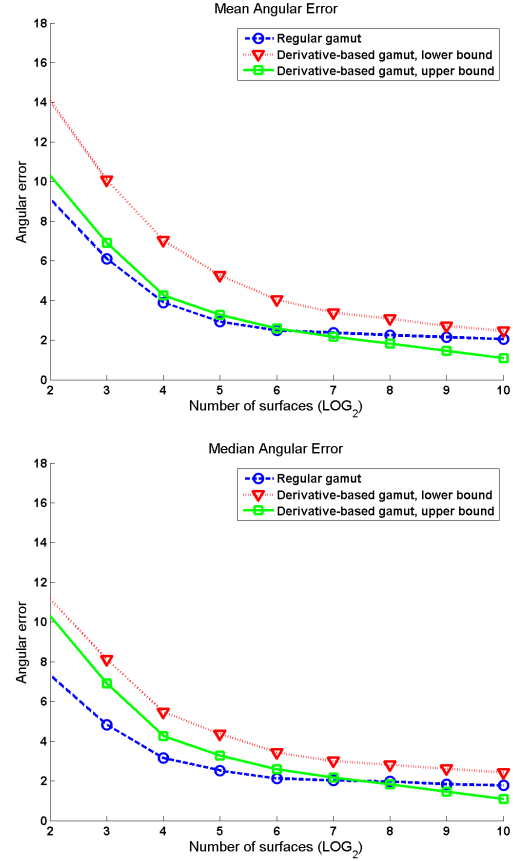


Figure 2. Results of experiment 1. The first figure shows the mean angular error over 1000 scenes for every number of surfaces, the second figure shows the median angular error.

$\frac{1}{2}n(n - 1)$  transitions, respectively. This process is repeated 1000 times, for  $n = \{4, 8, 16, 32, 64, 128, 256, 512, 1024\}$ .

In figure 2, results are shown for the regular gamut mapping algorithm and the derivative-based gamut mapping algorithm. The median and the mean angular error as function of the number of surfaces are shown. These graphs show that the regular gamut mapping slightly outperforms the derivative-based gamut mapping when the number of surfaces is small ( $\log_2(n) < \pm 6$ ). However, for a larger number of surfaces (and hence a larger number of edges), the derivative-based gamut mapping outperforms the regular gamut mapping. Note that the complexity of the two algorithms is comparable and the difference in runtime can be neglected.

### 5.2.2 Robustness against disturbing effects

The second experiment involves the robustness against diffuse light and deviations from the diagonal model, modelled by simulating an offset of the diagonal model (see

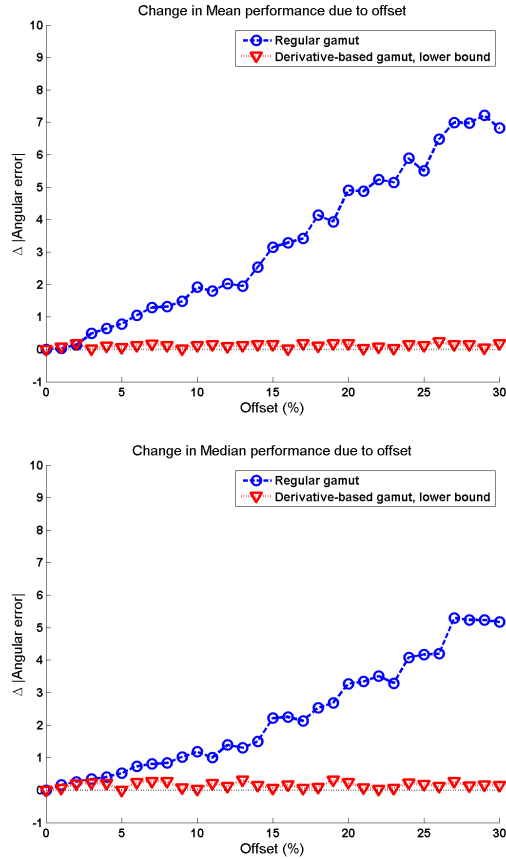


Figure 3. Results of experiment 2. The figures show the change in mean and median performance of the two algorithms. It can be seen that the error of the regular gamut mapping algorithm increases as the offset increases, while the derivative-based gamut mapping is not affected.

eq. (7)). For this experiment, the number of surfaces is kept fixed throughout the test. For each iteration,  $n = 8$  surfaces are generated by randomly selecting 8 reflectance spectra. These 8 surfaces are used to generate a scene with 8 edges, which is near the lower-bound on the number of edges. Next, instead of randomly selecting one illuminant spectra like the previous experiment, these spectra are combined with the canonical illuminant to form  $(R, G, B)$ -values. The diagonal-offset model is used to create the  $(R, G, B)$ -values under a different illuminant. The color of this illuminant is determined by applying the diagonal model to the canonical illuminant. The values of the elements of the diagonal matrix are randomly selected from the range  $[0.5 \dots 1.5]$ , and the offset is gradually increased, ranging from 0% of the average pixel value in the scene (*i.e.* no offset) to 30% of the average pixel value. So, a new  $(R_{\text{new}}, G_{\text{new}}, B_{\text{new}})$ -value is generated by randomly select-

ing a value in the range of:

$$R_{\text{new}} = \left[ \left( R - \frac{p}{100} x \right) \dots \left( R + \frac{p}{100} x \right) \right] \quad (16)$$

$$G_{\text{new}} = \left[ \left( G - \frac{p}{100} y \right) \dots \left( G + \frac{p}{100} y \right) \right] \quad (17)$$

$$B_{\text{new}} = \left[ \left( B - \frac{p}{100} z \right) \dots \left( B + \frac{p}{100} z \right) \right], \quad (18)$$

where  $(x, y, z)$  is the average pixel value in the scene (*i.e.* the average  $(R, G, B)$ -values of the 8 surfaces) and the offset is  $p\%$ .

In figure 3, the results are shown, relative to the performance without the simulation of the disturbing effects. From this experiment, it can be observed that by adding an offset to the diagonal model, the performance of the derivative-based gamut mapping algorithm is not affected, whereas the performance of the regular gamut mapping drops dramatically. The error increases linearly with the increasing offset.

In conclusion, the derivative-based method significantly outperforms the regular gamut mapping for simulated failure of the diagonal model and diffuse light.

### 5.3. Real data

The next experiments will be conducted on two sets of real images. The first consists of images taken under laboratory settings [2], the second set contains real-world images [5]. For these experiments, we follow the implementation of [13, 11]. We use the  $L_1$  norm maximization, for both the regular gamut and our derivative based gamut estimation. For the diagonal-offset model, we also use the  $L_1$  norm maximization of the diagonal transform while minimizing the  $L_1$  norm of the offset [11]. As a preprocessing step for regular gamut and diagonal-offset gamut, we use Gaussian averaging with the same scale to compute the derivatives for the derivative-based gamut. This procedure was found to improve the results for both the regular gamut and diagonal-offset gamut. To suppress high frequency noise amplification from the derivative operation, we compute the image derivatives with Gaussian derivative filters.

**SFU data set.** The images in this data set are all indoor scenes. There are 31 scenes, taken under 11 different light sources, resulting in a total of 321 images. For more information on this set, refer to [2].

The results of the regular gamut (RG), the regular gamut with the diagonal-offset model (RG+O) and the derivative-based gamut mapping (DG) on this data set are shown in table 1. From these results, it can be seen that the derivative-based gamut mapping algorithm performs similar to the regular gamut mapping algorithm and the regular gamut mapping with the diagonal-offset model [11]. Note that the regular gamut mapping algorithm could not find a solution for approximately 10% of the images, and the reported performance for this method only constitutes the images for which

Method	Mean	Median
RG - Performance on 288 images	4.5°	2.7°
RG+O	4.7°	3.1°
<b>Proposed: DG</b>	<b>4.7°</b>	<b>2.6°</b>
Grey-World	9.8°	7.0°
White-Patch	9.2°	6.5°
Shades of Grey	6.3°	3.9°
Color by Correlation	9.9°	6.8°

Table 1. Angular errors for several algorithms on the SFU data set, containing 321 images. Note that the regular gamut mapping algorithm (RG) did not find a solution for approximately 10% of the images in this set. The reported performance for the RG algorithm constitutes only those images for which a solution *was* found.

a solution *was* found. The regular gamut mapping with the diagonal-offset model and the derivative-based gamut mapping methods both found a solution for *all* images in the data set.

In conclusion, using the derivative-based gamut mapping on a data set with only few disturbing imaging factors does not deteriorate the performance compared to regular gamut mapping.

**Real-world data set.** This set consists of images that are captured using a camera with a grey sphere mounted on top. There are 15 different scenes, both indoor and outdoor, and each scene contains 10 images, resulting in a total of 150 image (see [5] for more information).

The results for this data set are shown in table 2. For this data set, the advantages of the derivative-based gamut mapping algorithm are more apparent. This data set is more challenging since it contains images recorded under difficult lighting settings like outdoor with a blue sky and bright sunlight. Hence, it can be expected that the proposed method performs better on such images than the regular gamut mapping, which can also be seen in table 2. The mean angular error for the proposed derivative-based gamut mapping is 6.7° compared to 7.2° for the regular gamut mapping and even 7.4° for the regular gamut mapping using the diagonal-offset model. Further, the median angular error of the proposed method is also lower.

To illustrate the output of the algorithms, results are shown in figure 4. The first image shows the original unprocessed image. The second image shows how the image looks like if the illuminant is perfectly estimated (for this purpose, the ground truth is used), and the third and fourth image depict the result of the derivative-based and regular gamut mapping algorithms, respectively.

## 6. Conclusion

In this paper, gamut mapping has been extended to incorporate higher-order statistics (derivatives) to estimate the illuminant. The use of higher-order statistics results in ro-

Method	Mean	Median
RG	7.2°	5.9°
RG+O	7.2°	6.1°
<b>Proposed: DG</b>	<b>6.7°</b>	<b>5.2°</b>
Grey-World	8.2°	7.3°
White-Patch	7.1°	6.7°

Table 2. Angular errors for several algorithms on the real-world data set.

bustness against deviations from the diagonal model and diffuse light which can be modelled by an offset of the image values

The derivative-based gamut mapping has the advantage over the diagonal-offset model [11] that position dependent (but low frequent) offsets are allowed. In the experimental section, we compared the proposed method with regular gamut mapping and the diagonal-offset model. On the SFU set all three methods obtained state-of-the-art results. On a more challenging set containing real-world images the proposed method outperformed the other approaches.

## References

- [1] K. Barnard. Improvements to gamut mapping colour constancy algorithms. In *European Conference on Computer Vision*, pages 390–403, 2000. 3
- [2] K. Barnard, L. Martin, B. Funt, and A. Coath. A data set for color research. *Color Research and Application*, 27(3):147–151, 2002. 4, 5, 6
- [3] D. Brainard and W. Freeman. Bayesian color constancy. *Journal of the Optical Society of America A*, 14:1393–1411, 1997. 1
- [4] G. Buchsbaum. A spatial processor model for object colour perception. *Journal of the Franklin Institute*, 310(1):1–26, July 1980. 1
- [5] F. Ciurea and B. Funt. A large image database for color constancy research. In *Proc. of the Eleventh Color Imaging Conference*, pages 160–164. IS&T - The Society for Imaging Science and Technology, 2003. 4, 6, 7
- [6] M. D’Zmura, G. Iverson, and B. Singer. Probabilistic color constancy. In *Geometric Representations of Perceptual Phenomena*, pages 187–202. Lawrence Erlbaum Associates, 1995. 1
- [7] G. Finlayson. Color in perspective. *IEEE Trans. on Pattern Analysis and Machine Intelligence*, 18(10):1034–1038, 1996. 3
- [8] G. Finlayson and S. Hordley. Improving gamut mapping color constancy. *IEEE Trans. on Image Processing*, 9(10):1774–1783, 2000. 3
- [9] G. Finlayson, S. Hordley, and P. Hubel. Color by correlation: a simple, unifying framework for color constancy. *IEEE Trans. on Pattern Analysis and Machine Intelligence*, 23(11):1209–1221, 2001. 1

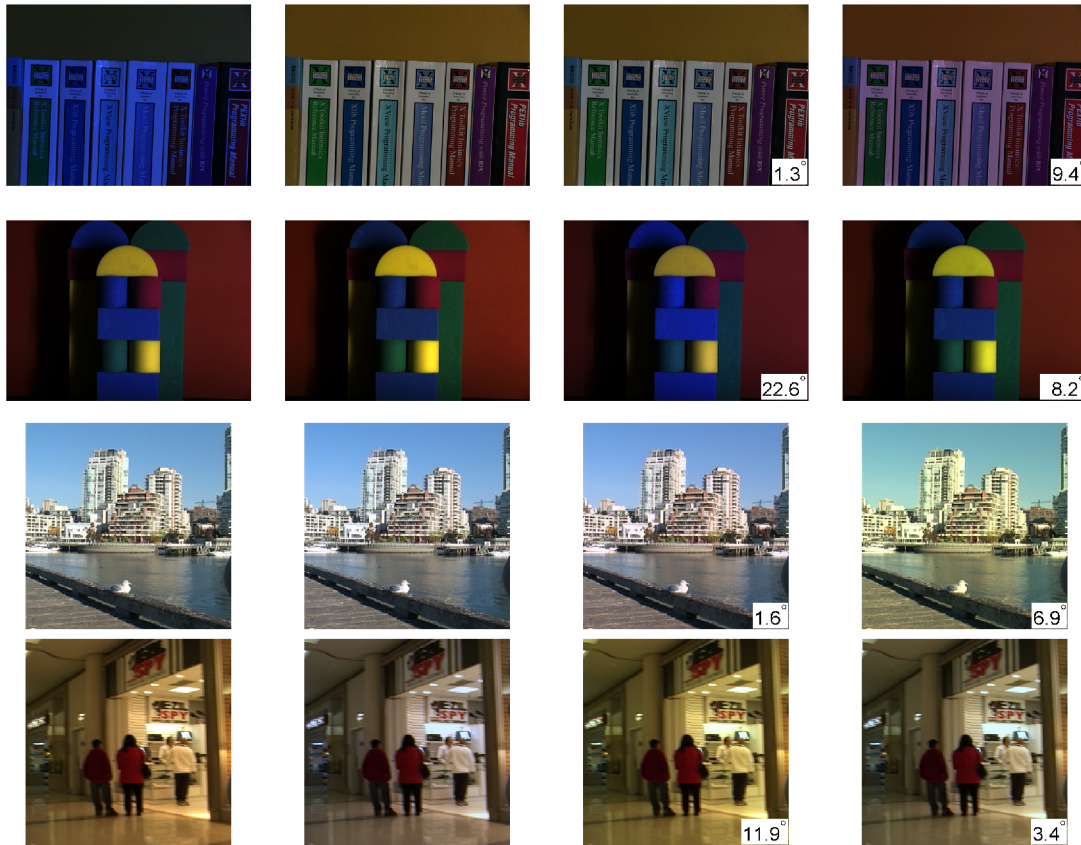


Figure 4. Examples of the results of the regular gamut mapping and the derivative-based gamut mapping. The original image is shown, followed by the result of perfect correction (using the ground truth), the result of the derivative-based gamut mapping and the result of the regular gamut mapping algorithm, respectively. The angular errors are displayed in the bottom right corner of the images.

- [10] G. Finlayson, S. Hordley, and I. Tasl. Gamut constrained illuminant estimation. *Int. Journal of Computer Vision*, 67(1):93–109, 2006. [1](#), [3](#)
- [11] G. Finlayson, S. Hordley, and R. Xu. Convex programming colour constancy with a diagonal-offset model. In *Proc. of IEEE Int. Conf. on Image Processing*, pages 948–951, 2005. [2](#), [3](#), [6](#), [7](#)
- [12] G. Finlayson and E. Trezzi. Shades of gray and colour constancy. In *Proc. of the Twelfth Color Imaging Conference*, pages 37–41. IS&T - The Society for Imaging Science and Technology, 2004. [1](#)
- [13] G. Finlayson and R. Xu. Convex programming color constancy. In *IEEE Workshop on Color and Photometric Methods in Computer Vision*, pages 1–8, 2003. [6](#)
- [14] D. Forsyth. A novel algorithm for color constancy. *Int. Journal of Computer Vision*, 5(1):5–36, 1990. [1](#), [3](#), [4](#)
- [15] T. Gevers and A. Smeulders. Pictoseek: combining color and shape invariant features for image retrieval. *IEEE Trans. Im. Proc.*, 9(1):102–119, 2000. [1](#)
- [16] S. Hordley. Scene illuminant estimation: past, present, and future. *Color Research and Application*, 31(4):303–314, 2006. [1](#)
- [17] S. Hordley and G. Finlayson. Reevaluation of color constancy algorithm performance. *Journal of the Optical Society of America A*, 23(5):1008–1020, 2006. [5](#)
- [18] E. Land. The retinex theory of color vision. *Scientific American*, 237(6):108–128, December 1977. [1](#)
- [19] S. Shafer. Using color to separate reflection components. *Color Research and Application*, 10(4):210–218, 1985. [1](#), [2](#)
- [20] J. van de Weijer, T. Gevers, and A. Gijsenij. Edge-based color constancy. *IEEE Trans. on Image Processing*, 16(9):2207–2214, 2007. [1](#)
- [21] J. von Kries. Influence of adaptation on the effects produced by luminous stimuli. In D. MacAdam, editor, *Sources of Color Vision*, pages 109–119. MIT Press, 1970. [2](#)